



Article

Synthesis of Mesoporous Silica Adsorbent Modified with Mercapto–Amine Groups for Selective Adsorption of Cu²⁺ Ion from Aqueous Solution

Sagar M. Mane ¹, Chaitany Jayprakash Raorane ^{2,*} and Jae Cheol Shin ^{1,*}¹ Division of Electronics and Electrical Engineering, Dongguk University-Seoul, Seoul 04620, Korea² School of Chemical Engineering, Yeungnam University, Gyeongsan 38541, Korea

* Correspondence: chaitanyaraorane22@gmail.com (C.J.R.); jcshin@dgu.ac.kr (J.C.S.)

Abstract: In a sol–gel co-condensation, a mesoporous silica hybrid integrated with (3-mercaptopropyl) trimethoxysilane (TMPSH) was prepared and then reacted with allylamine via a post-surface functionalization approach. Approximately 15 mol% of TMPSH was introduced into the mesoporous silica pore walls along with tetraethyl orthosilicate. The mercapto ligands in the prepared mesoporous silica pore walls were then reacted with allylamine (AM) to form the mercapto–amine-modified mesoporous silica adsorbent (MSH@MA). The MSH@MA NPs demonstrate highly selective adsorption of copper (Cu²⁺) ions (~190 mg/g) with a fast equilibrium adsorption time (30 min). The prepared adsorbent shows at least a five times more efficient recyclable stability. The MSH@MA NPs adsorbent is useful for selective adsorption of Cu²⁺ ions.

Keywords: silica nanoparticles; click chemistry; adsorption; aqueous solution; desorption



Citation: Mane, S.M.; Raorane, C.J.; Shin, J.C. Synthesis of Mesoporous Silica Adsorbent Modified with Mercapto–Amine Groups for Selective Adsorption of Cu²⁺ Ion from Aqueous Solution. *Nanomaterials* **2022**, *12*, 3232. <https://doi.org/10.3390/nano12183232>

Academic Editor: Carlos Lodeiro

Received: 31 August 2022

Accepted: 16 September 2022

Published: 18 September 2022

Publisher's Note: MDPI stays neutral with regard to jurisdictional claims in published maps and institutional affiliations.



Copyright: © 2022 by the authors. Licensee MDPI, Basel, Switzerland. This article is an open access article distributed under the terms and conditions of the Creative Commons Attribution (CC BY) license (<https://creativecommons.org/licenses/by/4.0/>).

1. Introduction

With the rapid development of the industrial sector, heavy metal pollutants are now considered a serious concern [1,2]. Toxic metal ions including copper, lead, mercury, etc., contaminate water bodies, and they induce severe biological and environmental toxicity [3,4]. With high solubility and bioaccumulation, copper ions (Cu²⁺) are considered toxic pollutants above a certain level. Copper poisoning can harm the immune system of living things, and cause disabilities to internal organs [5–8]. Among the various techniques available, adsorption is the most widely applied technique used for Cu²⁺ ion separation [9–13]. Designing novel adsorbent materials desirable for toxic metal ions adsorption is needed urgently. In general, porous materials are considered economically feasible. A range of materials including mesoporous carbon and silica materials are used for toxic metal ions adsorption [14–19]. Amongst these, mesoporous silica has proven significant adsorption efficiency due to its porous structure, high surface area, and recyclability [20–24]. Further, mesoporous silica materials offer the space to incorporate functional ligands to enhance adsorption capacity [25–27].

Mesoporous silica functionalized with mercapto groups (-SH) and amine groups (-NH₂) show a specific affinity for specific metal ions [28–31]. In general, increasing the ligand group content in adsorbent materials is thought to significantly improve the adsorption efficiency [32–34]. Sol–gel is the most simple, cost-effective, and very useful method to develop these kinds of materials. The co-condensation synthetic method offers the advantage of being able to introduce a high amount of organic functional ligand content in the mesopore walls [35–37].

In this work, we synthesize the mercapto–amine-groups-modified mesoporous silica adsorbent via a co-condensation method, and surface modification to increase the application efficiency of the adsorbent towards selective metal ions (Cu²⁺ ions). The synthesized mercapto–amine-grafted mesoporous silica adsorbent (MSH@MA NPs) was analyzed and

used to evaluate the removal capacity of Cu^{2+} ions from water. In addition, the adsorption characteristics of the prepared MSH@MA NPs adsorbent were evaluated by studying various parameters including pH, time, metal ion concentration, and recyclability. The study results suggest that the MSH@MA NPs could be used to selectively remove Cu^{2+} ions from contaminated water.

2. Materials and Methods

2.1. Chemicals

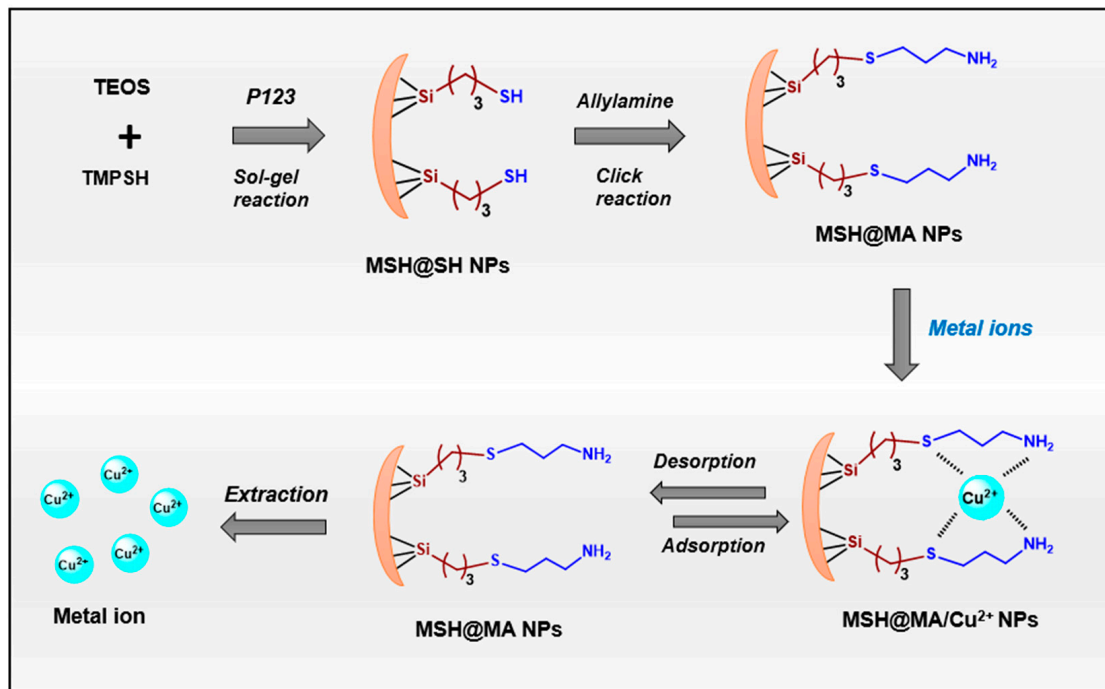
Pluronic P123 (average Mn 5800), (3-mercaptopropyl)trimethoxysilane (TMSPSH, 95%), tetraethoxysilane (TEOS, 98%), allylamine (AM, 98%), $\text{Cu}(\text{NO}_3)_2 \cdot 3\text{H}_2\text{O}$ (98%), $\text{Cd}(\text{NO}_3)_2 \cdot 4\text{H}_2\text{O}$ (98%), $\text{Pb}(\text{NO}_3)_2$ (99%), $\text{Cr}(\text{NO}_3)_3 \cdot 6\text{H}_2\text{O}$, tetrahydrofuran (THF), hydrochloric acid (HCl), ethanol, and deionized water were received from Aldrich Chemicals, St. Louis, MO, USA. All the metal ion stock solution was prepared with 100 mg/mL by dissolving the appropriate amount of each metal salt in a neutral pH (pH 7) buffer and stored at 4 °C.

2.2. Synthesis of MSH@SH NPs

For the synthesis of MSH@SH NPs, first, the (3-mercaptopropyl)trimethoxysilane (TMSPSH)-groups-incorporated mesoporous silica was created via co-condensation method using Pluronic P123 as structure-directing templating agent. To form a clear solution, P123 (1 g) was dissolved in deionized water (40 mL) containing 3 g HCl under magnetic agitation for 2 h at 37 °C. The pre-mixed TMPSH and TEOS solution [TMPSH/(TEOS + TMPSH) = 15 mol%] was slowly added to this, and the solution was agitated for 24 h at 40 °C, and further heated at 90 °C. The obtained precipitate was filtered, washed with water, and dried at 60 °C. The surfactant was extracted by stirring with an acidified ethanolic solution (1 mL HCl in 50 EtOH). The extraction procedure was carried out three times. MSH@SH NPs was the name given to the extracted surfactant sample (Scheme 1). Second, the mercapto groups in the MSH@SH sample were further modified with allylamine (AM) groups (5 mL, 0.2 M) by incubating the MSH@SH NPs (0.2 g) in ethanol (20 mL) for 24 h at 55 °C [38]. The finished product was filtered, washed with THF and ethanol, and dried at 60 °C. MSH@MA NPs was the name given to the mercapto-amine-modified mesoporous silica adsorbent (Scheme 1). For comparison, we prepared control MSNs without any ligand functionalities such as mercapto-amine (MA) groups. For the synthesis of a control sample, about 1 g of P123 was dissolved in deionized water (40 mL) containing 3 g HCl under magnetic agitation for 2 h at 37 °C. To this, TEOS solution (1.5 mL) was added, and the solution was magnetically stirred for 24 h at 40 °C and further heated at 90 °C. The obtained precipitate was filtered, washed with water, and dried at 60 °C. The surfactant was extracted by stirring with an acidified ethanolic solution (1 mL HCl in 50 EtOH). The obtained sample was named as MSNs.

2.3. Characterization

Fourier-transform infrared (FT-IR, JASCO FTIR 4100, Easton, MD, USA) spectra were carried out using the KBr pelleting method. X-ray diffraction (XRD, Bruker AXN, Billerica, MA, USA) analysis was performed with CuK radiation. Nitrogen adsorption-desorption experiments were carried out on a Nova 4000e analyzer (Quantachrome Instruments, Boynton Beach, FL, USA) at −196 °C. The surface area, pore size, and pore volumes were calculated using the Brunauer-Emmett-Teller (BET) and Barrett-Joyner-Halenda (BJH) techniques, respectively. Scanning electron microscopy (SEM, JEOL 6400, Akishima, Tokyo, Japan) was performed with a 10 kV accelerating voltage. A transmission electron microscope (TEM) analysis was performed on a JEOL 2010 TEM, Akishima, Tokyo, Japan at 200 kV. The materials were subjected to thermogravimetric (TG, Perkin-Elmer Pyris 1, Waltham, MA, USA) analysis at a heating rate of 10 °C/min. An inductively coupled plasma atomic emission spectrometer was used to quantify adsorbed metal ions (ICP-AES, Perkin-Elmer, Model Optima 5300 DV, Waltham, MA, USA).



Scheme 1. Schematic representation for the synthesis of MSH@MA NPs adsorbent.

2.4. Adsorption Study

The following equations were applied to determine the amounts of an adsorbed metal ion at equilibrium (Q_e , mg/g) and at time t (Q_t , mg/g).

$$Q_e = [(C_0 - C_e)V]/m \quad (1)$$

$$Q_t = [(C_0 - C_t)] V/m \quad (2)$$

where C_0 and C_e are the initial and equilibrium concentrations, respectively, and C_t is the concentration at any given time t ; V is the volume of solution (mL), and m is the adsorbent weight (g).

2.4.1. Effect of pH

To carry out this study, MSH@MA NPs sample (0.1 g) was suspended in a 10 mL buffer solution and about 0.5 mL of Cu^{2+} ion solution (100 mg/L) was introduced. Further, the solution medium was adjusted with different pH levels (3, 5, 6.5, 7, and 9) using 0.1 M HCl, and shaken at 25 °C for 60 min to reach equilibrium. The sample was isolated by filtration, and the obtained filtrate solution was used to determine unadsorbed Cu^{2+} ions using the ICP-AES instrument.

2.4.2. Effect of Time

A kinetic adsorption study was performed at different time points. For this study, the MSH@MA NPs sample (0.1 g) was suspended in water (10 mL), and the medium pH was adjusted. Cu^{2+} ion solution (0.5 mL) was introduced and agitated at 25 °C for different lengths of time (5–120 min). After the specified time, the sample was filtered and washed with water. ICP-AES analysis was performed on the filtrate obtained.

2.4.3. Effect of Competitive Metal Ions

For this study, the MSH@MA NPs sample (0.1 g) was suspended in a vial containing 10 mL of a mixed solution containing Cu^{2+} and Co^{2+} , Cd^{2+} , Pb^{2+} , and Cr^{3+} ions, and then agitated at 25 °C for 60 min. Finally, ICP-AES analysis was used to determine the number of metal ions adsorbed.

2.4.4. Recyclability Test

To accomplish this study, metal-adsorbed MSH@MA/Cu²⁺ NPs sample (0.1 g) was agitated for 60 min at 25 °C in 10 mL of aqueous HCl solution (0.1 M). The sample was filtered, washed several times, and dried at 60 °C. The desorbed metal ion was determined. The adsorption–desorption procedure was repeated five times in a row, with the adsorption efficiency of the MSH@MA NPs being determined each time.

3. Results and Discussion

3.1. FTIR Analysis

The FTIR spectrum of mercapto-amine-groups-functionalized mesoporous silica MSH@MA NPs is shown in Figure 1a. The stretching modes at 594, 2622, 2895, and 2932 cm^{−1}, are assigned to the stretching modes of the alkyl (−CH₂−CH₂−) stretching peaks, evidencing that the mercapto-amine groups are present in the silica materials [39,40]. In addition, the typical band at 965 and 1088 cm^{−1} promotes the formation of surface silanol and siloxane networks in MSH@MA NPs. Moreover, the control MSNs show at 965 cm^{−1} and 1088 cm^{−1}, depicting surface silanol and siloxane groups, without any specific peaks for organic ligand mercapto-amine groups (Figure 1b).

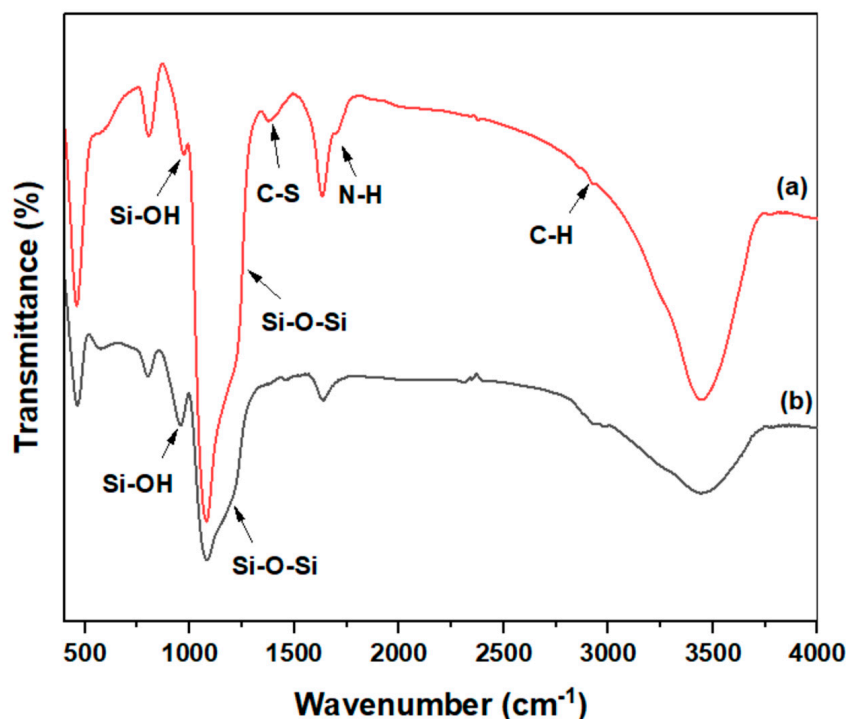


Figure 1. FTIR spectra of the (a) MSH@MA NPs; (b) MSNs.

3.2. XRD and BET Analysis of MSH@MA NPs

Figure 2a depicts the powder XRD pattern of the mercapto-amine-groups-functionalized MSH@MA NPs. The sample shows the diffraction peak at $2\theta = 0.97^\circ$, indicating (100) diffraction that indicates the formation of an ordered mesostructure arrangement in the MSH@MA NPs, as shown in Figure 2a. A similar XRD pattern is also observed for the control samples (See Figure S1 in Supplementary Materials). Figure 2b shows type IV isotherm curves with H1 hysteresis of the MSH@MA NPs sample, indicating mesopore formation [41]. The MSH@MA NPs sample's surface area, pore volume, and mesopore size are determined to be approximately 563 m²/g, 0.61 cm³/g, and 2.7 nm, respectively. For the control MSNs, the estimated surface area, pore volume, and average mesopore size are determined to be 690 m²/g, 0.72 cm³/g, and 3.1 nm, respectively (See Figure S2a in Supplementary Materials).

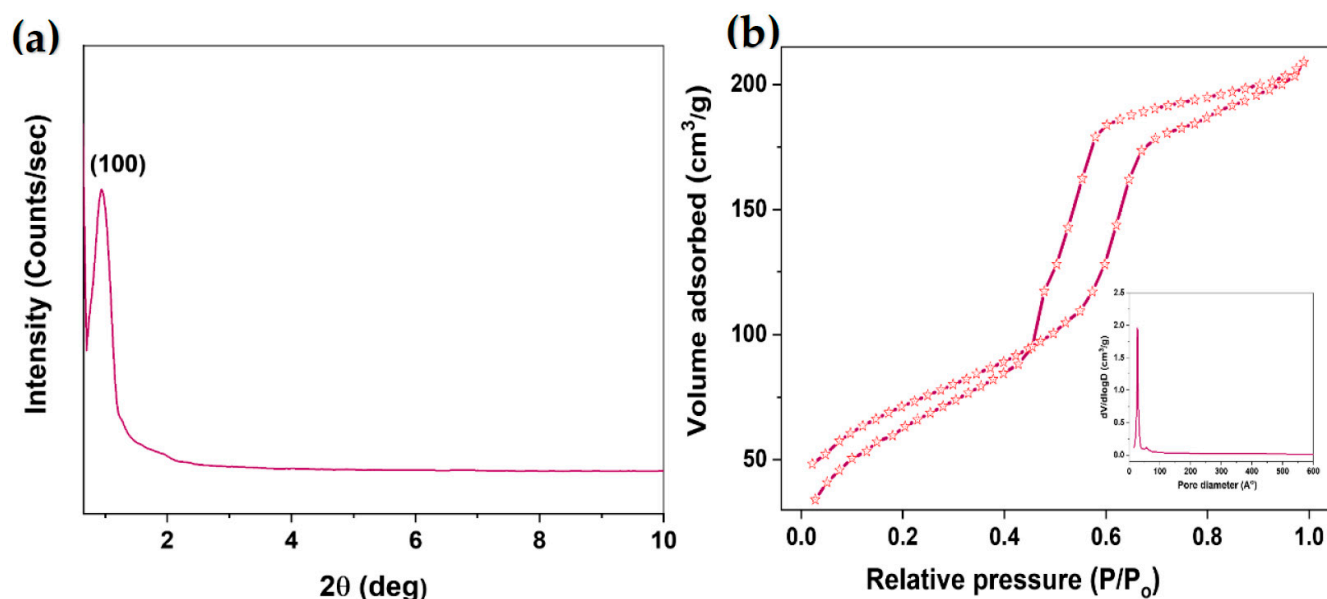


Figure 2. Structural and surface area analysis. (a) Low-angle XRD pattern of the MSH@MA NPs. (b) N₂ adsorption–desorption isotherm and pore size distribution (inset figure) of the MSH@MA NPs.

3.3. TGA, Zeta, and Particle Size Analysis of MSH@MA NPs

The TG analysis of the MSH@MA NPs is shown in Figure 3a. As shown in Figure 3a, the MSH@MA NPs sample experiences an initial weight loss of about 2.3 wt% at 100 °C, due to surface-adsorbed moisture evaporation. Following that, a 20.8 wt% weight loss occurs at 101–650 °C, indicating that the functionalized ligand decomposes. The control MSNs sample shows a negligible weight loss, with an overall weight loss of about ~2.8 wt% caused by physisorbed moisture (See Figure S3a). As shown in Figure 3b, the MSH@MA NPs sample has positive zeta potential values of about $+16 \pm 1$ mV, $+10 \pm 2$ mV, and $+7 \pm 1$ mV at pH 3, 5, and 6 respectively. In addition, the zeta potential values at pH 7 and 9 are about -15 ± 1 and -21 ± 2 mV, respectively, and the negative zeta potential value arises due to the presence of sulfur atom in the modified functional groups, which supports the existing mercapto–amine ligands in the MSH@MA NPs adsorbents [42]. The control sample shows negative zeta potential values of about -6 to -24 mV at pH 3 to 9, respectively, indicating the presence of negatively charged silanol groups (Figure 3b). Furthermore, the particle size analysis of MSH@MA NPs measured by DLS analysis reveals particle sizes fall in between the 100 to 400 nm range, with the average particle size of about $\sim 250 \pm 100$ nm (Figure 3c). In contrast, MSNPs show particle sizes in the range from ~ 100 nm to 500 nm, with an average particle size of about ~ 300 nm (See Figure S3b).

3.4. Morphological Analysis (SEM and TEM) of MSH@MA NPs

SEM images of MSH@MA NPs reveal aggregated particles with an average size of 400 nm, as shown in Figure 4a. The TEM image (Figure 4b) shows the mesopore arrangement in the MSH@MA NPs sample, evidencing the existence of ordered mesopore structures. The presence of wormhole-like porous structure can be easily noticed from the TEM analysis. SEM and TEM (inset) images of the MSNs sample also show aggregated particles with a particle size of about 350 nm, with clear mesopore channels (See Figure S2b, ESI).

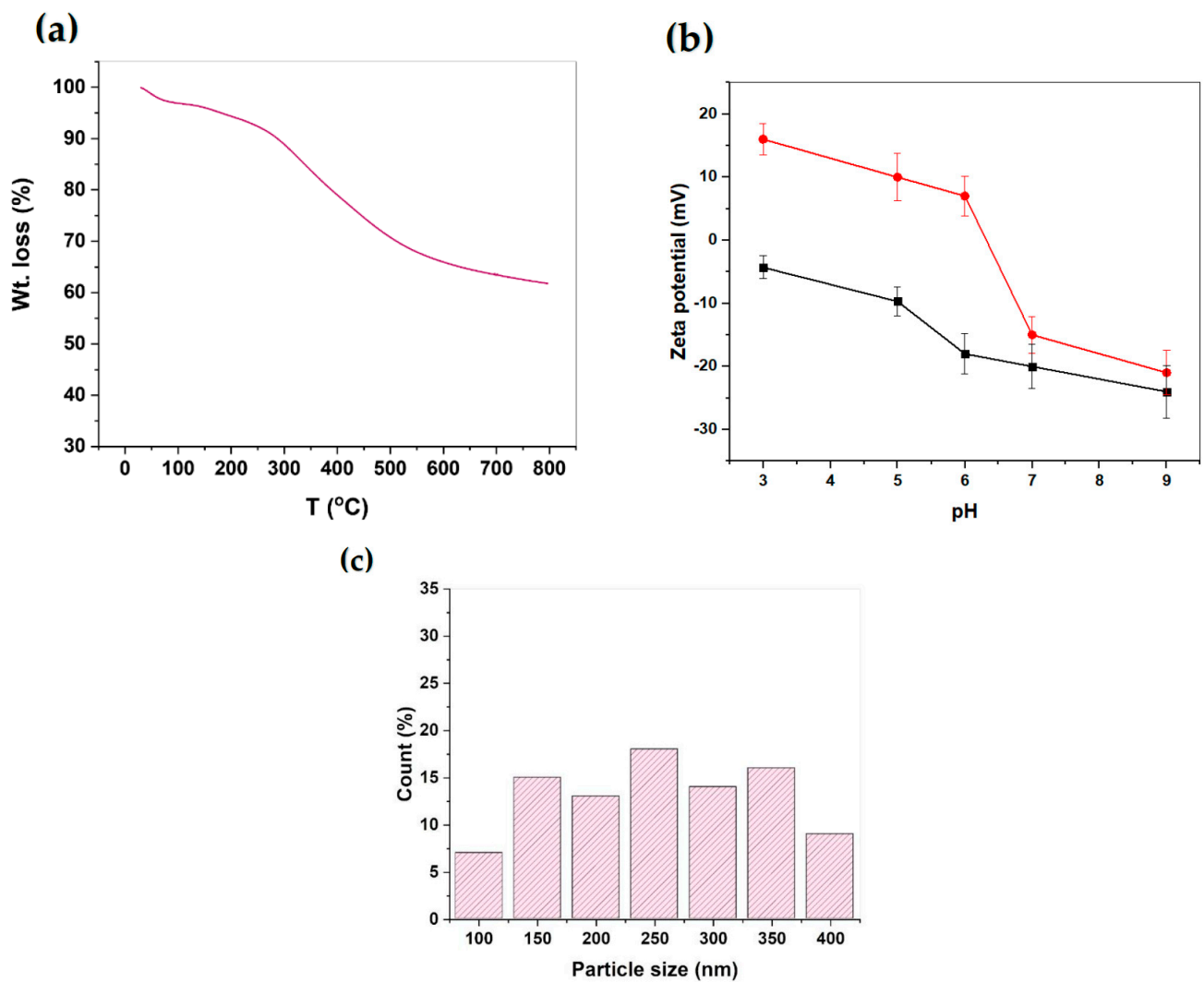


Figure 3. (a) TG analysis of MSH@MA NPs. (b) Zeta potential of MSH@MA NPs (red line) and MSNs (black line). (c) Particle size distribution of the MSH@MA NPs.

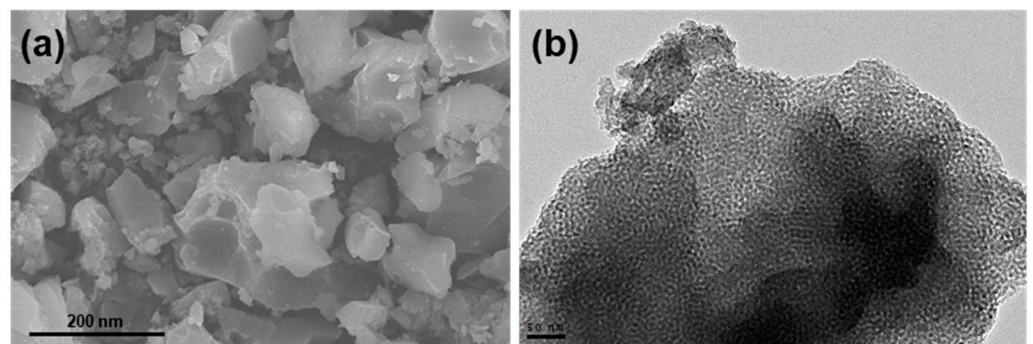


Figure 4. Morphological analysis (a) SEM; and (b) TEM images of the MSH@MA NPs.

3.5. Adsorption Kinetics

3.5.1. Effect of pH and Time on Adsorption Efficacy of MSH@MA NPs

Adsorption medium pH-based adsorption was studied at different pH conditions. Figure 5a shows that the Cu^{2+} ion adsorption gradually increases from pH 3 to pH 7, and then decreases further while reaching pH 9. The maximum of Cu^{2+} ions adsorption is achieved at pH 6.5, the estimated amount being 190 mg/g (Figure 5b). Therefore, pH 6.5

was selected for further kinetic studies. Furthermore, the MSH@MA NPs show enhanced adsorption in the pH 3 to 7 range, indicating that the surface-modified mercapto–amine groups effectively increase the adsorption efficiency of the MSH@MA NPs. The adsorption capacity of Cu^{2+} ions decreases at a low pH due to lower metal ion–ligand affinity. This might be caused due to the interference of H^+ ions and the Cu^{2+} ions under reduced pH [43]. The adsorption efficiency of MSH@MA NPs towards Cu^{2+} ions is greatly decreased at low pH conditions such as pH 3 and pH 5. At these reduced pH conditions, the concentration of acidic protons (H^+ ions) in the solution medium is considerably higher and it could competitively interact with the nitrogen (N) and sulfur (S) atoms. Thus, the Cu^{2+} ion interaction with these mercapto–amine ligand groups is considerably hindered. This is the reason why the Cu^{2+} ions are adsorbed at a low amount by the MSA@MA NPs under acidic pH conditions [44].

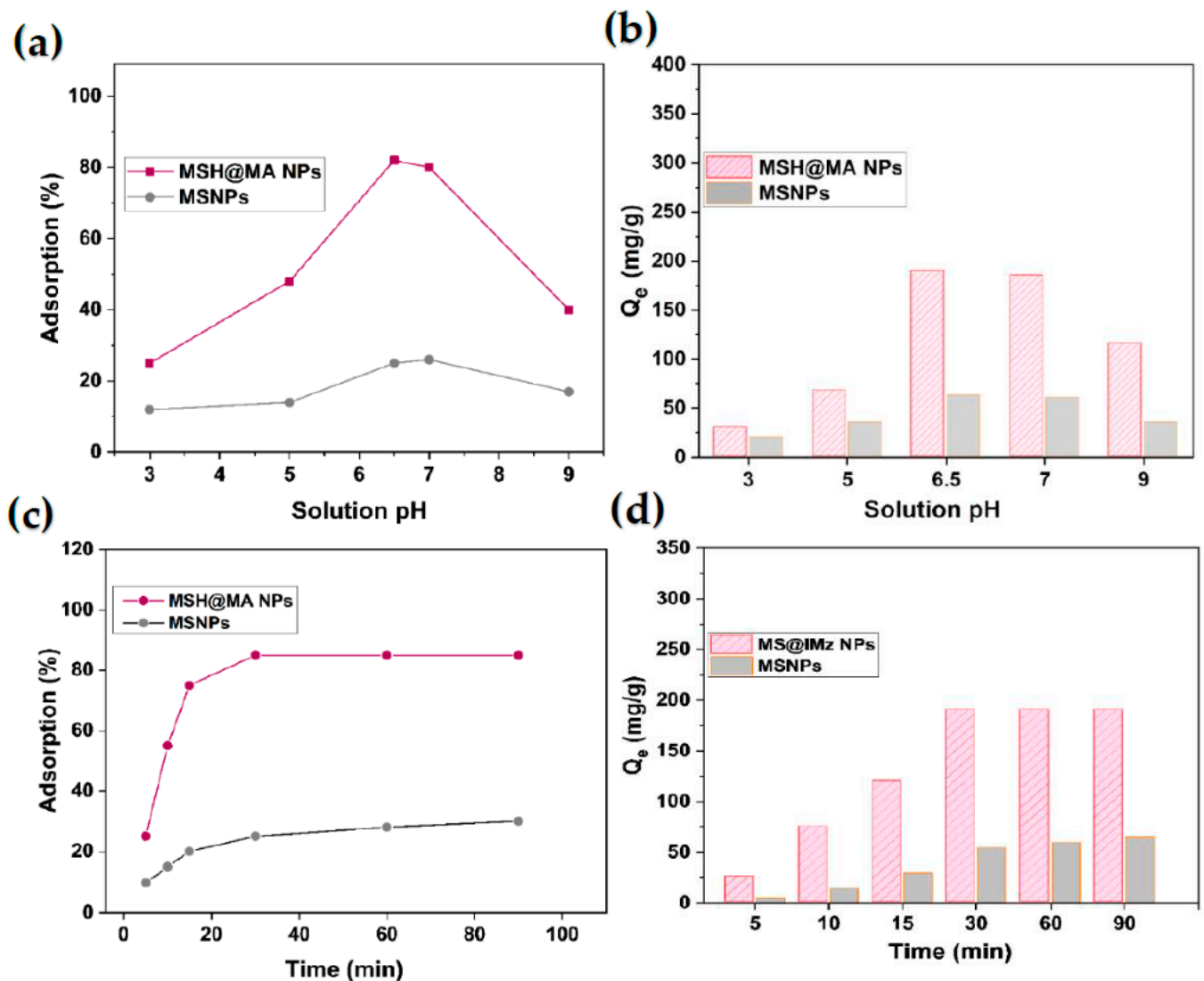


Figure 5. Adsorption kinetics of MSH@MA NPs. (a) Influence of solution pH on the adsorption percentage of Cu^{2+} ions onto the MSH@MA NPs. (b) Influence of solution pH on the amount of adsorption of Cu^{2+} ions onto the MSH@MA NPs. (c) Influence of contact time on the adsorption percentage of Cu^{2+} ions onto the MSH@MA NPs. (d) Influence of contact time on the amount of adsorption of Cu^{2+} ions onto the MSH@MA NPs.

Time-dependent adsorption kinetics were calculated using a Cu^{2+} ion solution containing 100 mg/L. Figure 5c shows that the adsorption efficiency of MSH@MA NPs on Cu^{2+}

ions increases before reaching equilibrium. The prepared MSH@MA NPs takes a short time to reach maximum adsorption of 190 mg/g, with approximately 85% of adsorption occurring within 30 min, and reaching equilibrium adsorption in about 60 min, and almost reaching equilibrium when increasing the time to 90 min (Figure 5d).

3.5.2. Effect of Adsorbent Dosage and Selective Efficiency of MSH@MA NPs

The adsorption behavior of the prepared MSH@MA NPs was tested at 25 °C with different amounts of adsorbent (10–150 mg/L) using Cu²⁺ ions (100 mg/L). Figure 6a shows that increasing the quantity of MSH@MA NPs increases the Cu²⁺ ion adsorption. As shown in the graph, using adsorbent amounts of 100 mg/L, approximately 85% of the removed Cu²⁺ ions are adsorbed. The obtained results reveal that the quantity of mercapto–amine groups increases with increasing the adsorbent dosage of 150 mg/L, and the functionalities are responsible for the Cu²⁺ ion removal from the aqueous solution.

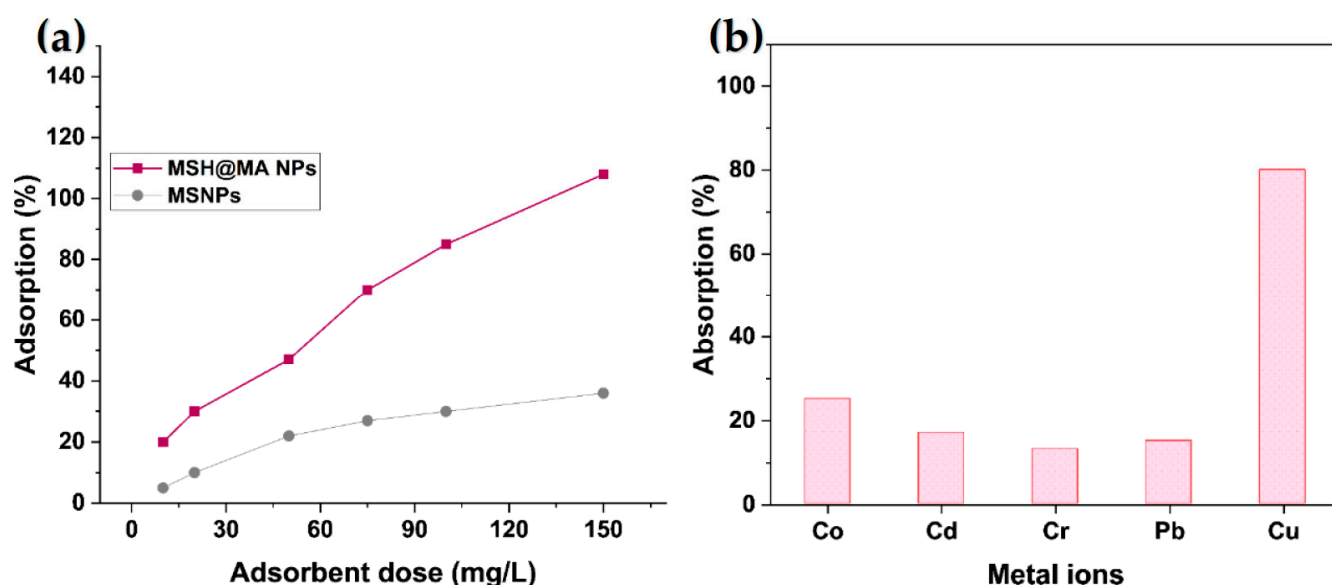


Figure 6. (a) Effect of adsorbent dosage of Cu²⁺ ions onto the MSH@MA and MS NPs. (b) Selective adsorption efficiency for various competitive metal ions by MSH@MA NPs.

The selectivity of the adsorbent was studied along with the competitive metal ions. As shown in Figure 6b, the MSH@MA NPs sample exhibits more Cu²⁺ ion adsorption than the other metal ions. According to these findings, other competitive metal ions do not interfere with the modified functional groups on the MSH@MA NPs, and do not cause any notable adsorption efficiency toward the selective adsorption of Cu²⁺ ions. This implies that the mercapto–amine functional groups in MSH@MA NPs have a preferable affinity for Cu²⁺ ions than the other ions [23,44]. This is due to the interaction between Cu²⁺ ions and mercapto–amine being stronger than those between other metal ions and mercapto–amine ligands. Therefore, the higher selectivity of MSH@MA NPs towards Cu²⁺ ions is due to the fact that the softer transition metal ions (for example, Cu²⁺) are prone to form stable complexes with ligands carrying softer donor atoms [45].

3.5.3. Adsorption Kinetics in Aqueous Solution and Recyclability of MSH@MA NPs

The adsorption of Cu²⁺ ions fit well with a pseudo-second-order kinetic equation in Figure 7a, and the constant K_{ad} is estimated to be 3.9×10^{-3} g/mg/min and 4.8×10^{-3} g/mg/min for initial concentrations of 50 and 100 mg/L of Cu²⁺ ions, respectively (Table 1). The correlation coefficients (R^2) for the Langmuir model are larger and fit better than the Freundlich model, indicating that the Cu²⁺ ions adsorption of the functional groups could be described as monolayer adsorption (Table 2). According to Table 3, the maximum

adsorption capacity of MSH@MA NPs for Cu^{2+} is determined to be 190 mg/g, which is higher than the various types of adsorbents previously reported [43–50].

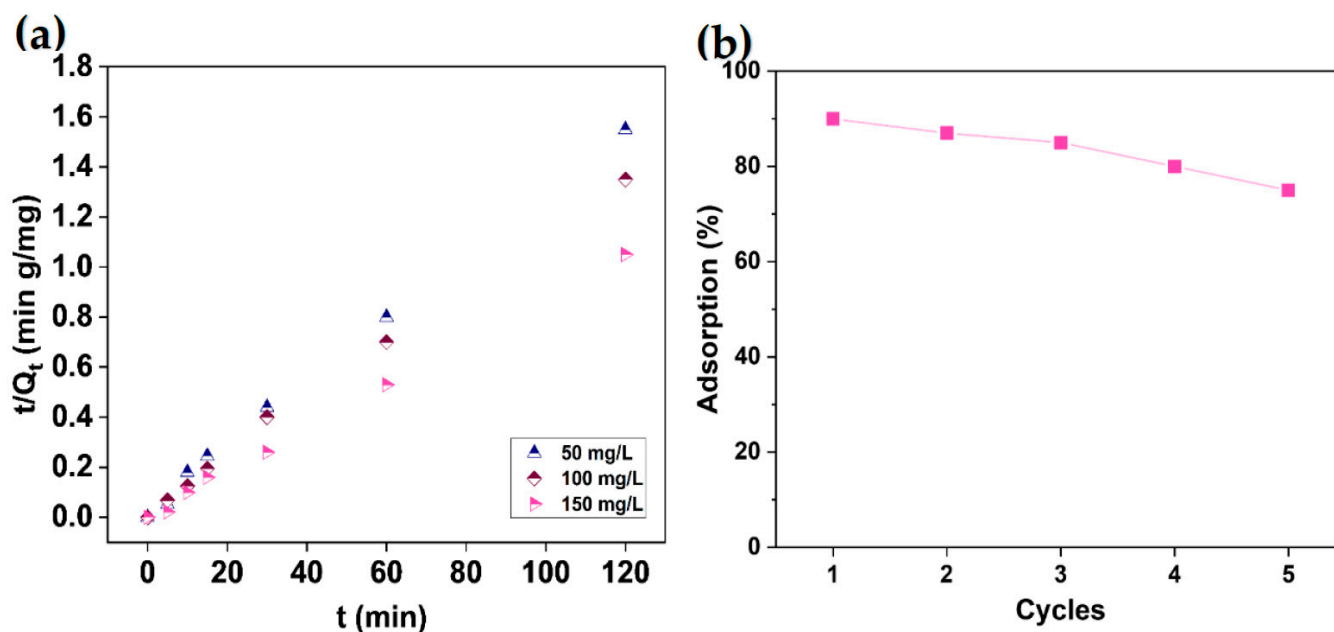


Figure 7. (a) Adsorption kinetics of the MSH@MA NPs in an aqueous solution of Cu^{2+} ions at an initial concentration of 50, 100, and 150 mg/L, respectively. (b) Adsorption–desorption efficiency towards Cu^{2+} ions in different cycles by MSH@MA NPs.

Table 1. The pseudo-second-order rate constant of adsorption kinetics of MSH@MA NPs in an aqueous solution of Cu^{2+} ions.

Initial Conc. of Metal Ions (mg/L)	K_{ad} (g/mg/min)	R^2
50	Cu^{2+}	Cu^{2+}
	2.8×10^{-3}	0.98
	100	0.97
150	4.8×10^{-3}	0.97

Table 2. Comparison of Langmuir and Freundlich isothermal adsorption-related parameters of the MSH@MA NPs materials for Cu^{2+} ions.

	Langmuir		Freundlich			
	Q_m (mg/g)	K_L (L/mg)	R^2	$1/n$	K_F ((mg/g)/(mg/mL))	R^2
MSH@MA NPs/ Cu^{2+}	190	7.85	0.98	1.73	4.8	0.95

The recyclability and reusability of the prepared MSH@MA NPs were determined. For this study, 0.1 g of Cu^{2+} ions adsorbed MSH@MA NPs was treated with 0.1 M HCl (25 mL) and stirred for 60 min before centrifuging, washing with water, and drying. The adsorption capacity of the recycled sample was then tested by adsorbing the Cu^{2+} ions from the solution and determining the adsorbed metal ions. Figure 7b depicts the adsorption capacity maintained at about 95–80% in the subsequent three cycles, revealing the MSH@MA NPs' retention of Cu^{2+} ions adsorption capacity.

Table 3. Comparison of the adsorption capacity of the various functional adsorbent materials.

Type of Adsorbent	Adsorption _{max} (mg/g)	Reference
Sulfur-functionalized silica microspheres	62.3	[43]
Amino-functionalized mesoporous silica	36.4	[44]
Mesoporous silica SBA-15-triethylenetetramine	23.9	[45]
Multi-modified granulated SBA-15	31.8	[46]
Dopamine-functionalized silica NPs	58.7	[47]
Fe ₃ O ₄ @SiO ₂ nanoparticles	51.04	[48]
Chitosan–carboxymethyl starch composite	95	[49]
Chitosan@TiO ₂ composites	31	[50]
Mercapto–amine-modified mesoporous silica adsorbent	190	This work

4. Conclusions

In this study, mercapto–amine-groups-modified MSH@MA NPs were synthesized via thiolene click reaction for selective removal of Cu²⁺ ions. By this approach, enriched mercapto–amine functional groups were incorporated into the silica surfaces, which show selectivity towards Cu²⁺ ions. The experimental results reveal that solution pH, adsorption time, metal ion concentration, and adsorbent dosage all have a significant impact on adsorption behavior. At 25 °C, the prepared MSH@MA NPs have an estimated adsorption capacity of 190 mg/g of Cu²⁺ ions. The experimental adsorption results show that functionalized mercapto–amine groups in MSH@MA NPs have significantly higher adsorption activity towards Cu²⁺ ions. As a result, the MSH@MA NPs could be used to selectively remove Cu²⁺ ions from an aqueous solution.

Supplementary Materials: The following supporting information can be downloaded at: <https://www.mdpi.com/article/10.3390/nano12183232/s1>, Figure S1: XRD analysis of control MSNs sample; Figure S2: (a) N₂ sorption analysis; and (b) SEM and TEM (inset) images of control MSNs sample; Figure S3: (a) TGA; and (b) DLS analysis of control MSNs sample.

Author Contributions: Conceptualization, S.M.M. and C.J.R.; methodology, S.M.M. and C.J.R.; software, C.J.R.; validation, S.M.M. and C.J.R.; formal analysis, C.J.R.; investigation, S.M.M.; resources, C.J.R.; data curation, S.M.M. and C.J.R.; writing—original draft, S.M.M., C.J.R. and J.C.S.; writing—review and editing, S.M.M. and C.J.R.; visualization, J.C.S.; supervision, J.C.S.; project administration, J.C.S.; funding acquisition, J.C.S. All authors have read and agreed to the published version of the manuscript.

Funding: This study was supported by the National Research Foundation of Korea (NRF-2019M3F5A1A01077146, NRF-2020R1A2C1015206, and NRF-2021M3H4A1A02051331).

Data Availability Statement: Not applicable.

Conflicts of Interest: The authors declare no conflict of interest.

References

1. Ali, I. New generation adsorbents for water treatment. *Chem. Rev.* **2012**, *112*, 5073–5091. [[CrossRef](#)] [[PubMed](#)]
2. Yang, Q.; Li, Z.Y.; Lu, X.N.; Duan, Q.N.; Huang, L.; Bi, J. A review of soil heavy metal pollution from industrial and agricultural regions in China: Pollution and risk assessment. *Sci. Total Environ.* **2018**, *642*, 690–700. [[CrossRef](#)] [[PubMed](#)]
3. Chu, Z.J.; Fan, X.H.; Wang, W.N.; Huang, W.C. Quantitative evaluation of heavy metals' pollution hazards and estimation of heavy metals' environmental costs in leachate during food waste composting. *Waste Manag.* **2019**, *84*, 119–128. [[CrossRef](#)] [[PubMed](#)]
4. Schwarzenbach, R.P.; Escher, B.I.; Fenner, K.; Hofstetter, T.B.; Johnson, C.A.; Gunten, U.V.; Wehrli, B. The challenge of micropollutants in aquatic systems. *Science* **2006**, *313*, 1072–1077. [[CrossRef](#)] [[PubMed](#)]
5. Moorthy, M.S.; Cho, H.-J.; Yu, E.-J.; Jung, Y.-S.; Ha, C.-S. A modified mesoporous silica optical nanosensor for selective monitoring of multiple analytes in water. *Chem. Commun.* **2013**, *49*, 8758–8760. [[CrossRef](#)] [[PubMed](#)]

6. Nagappan, S.; Choi, M.-C.; Sung, G.; Park, S.S.; Moorthy, M.S.; Chu, S.-W.; Lee, W.-K.; Ha, C.-S. Highly transparent, hydrophobic fluorinated polymethylsiloxane/silica organic-inorganic hybrids for anti-stain coating. *Macromol. Res.* **2013**, *21*, 669–680. [[CrossRef](#)]
7. Lubick, N.; Malakoff, D. With pact's completion, the real work begins. *Science* **2013**, *341*, 1443–1445. [[CrossRef](#)] [[PubMed](#)]
8. Bose-O'Reilly, S.; McCarthy, K.M.; Steckling, N.; Lettmeier, B. Mercury exposure and children's health. *Curr. Probl. Pediatr. Adolesc. Health Care* **2010**, *40*, 186–215. [[CrossRef](#)] [[PubMed](#)]
9. Bessbousse, H.; Rhlalou, T.; Verchère, J.F.; Lebrun, L. Novel Metal-Complexing Membrane Containing Poly(4-vinylpyridine) for Removal of Hg(II) from Aqueous Solution. *J. Phys. Chem. B* **2009**, *113*, 8588–8598. [[CrossRef](#)] [[PubMed](#)]
10. Moorthy, M.S.; Seo, D.-J.; Song, H.-J.; Park, S.S.; Ha, C.-S. Magnetic mesoporous silica hybrid nanoparticles for highly selective boron adsorption. *J. Mater. Chem. A* **2013**, *1*, 12485–12496. [[CrossRef](#)]
11. Veglio, F.; Beolchini, F. Removal of metals by biosorption: A review. *Hydrometallurgy* **1997**, *44*, 301–316. [[CrossRef](#)]
12. Moorthy, M.S.; Kim, M.-J.; Bae, J.-H.; Park, S.S.; Saravanan, N.; Kim, S.-H.; Ha, C.-S. Multifunctional Periodic Mesoporous Organosilicas for Biomolecule Recognition, Biomedical Applications in Cancer Therapy, and Metal Adsorption. *Eur. J. Inorg. Chem.* **2013**, *2013*, 3028–3038. [[CrossRef](#)]
13. Miretzky, P.; Cirelli, A.F. Hg(II) removal from water by chitosan and chitosan derivatives: A review. *J. Hazard. Mater.* **2009**, *167*, 10–23. [[CrossRef](#)] [[PubMed](#)]
14. Davidescu, C.-M.; Ardelean, R.; Popa, A. New polymeric adsorbent materials used for removal of phenolic derivatives from wastewaters. *Pure Appl. Chem.* **2019**, *91*, 443–458. [[CrossRef](#)]
15. Moorthy, M.S.; Tapaswi, P.K.; Park, S.S.; Mathew, A.; Cho, H.-J.; Ha, C.-S. Ion-imprinted mesoporous silica hybrids for selective recognition of target metal ions. *Micropor. Mesopor. Mater.* **2013**, *180*, 162–171. [[CrossRef](#)]
16. Tapaswi, P.K.; Moorthy, M.S.; Park, S.S.; Ha, C.-S. Fast, selective adsorption of Cu²⁺ from aqueous mixed metal ions solution using 1,4,7-triazacyclononane modified SBA-15 silica adsorbent (SBA-TACN). *J. Solid State Chem.* **2014**, *211*, 191–199. [[CrossRef](#)]
17. Lu, X.; Wang, F.; Li, X.-Y.; Shih, K.; Zeng, E.Y. Adsorption and Thermal Stabilization of Pb²⁺ and Cu²⁺ by Zeolite. *Ind. Eng. Chem. Res.* **2016**, *55*, 8767–8773. [[CrossRef](#)]
18. Park, S.S.; Moorthy, M.S.; Ha, C.-S. Periodic mesoporous organosilicas for advanced applications. *NPG Asia Mater.* **2014**, *6*, e96. [[CrossRef](#)]
19. Parida, D.; Salmeia, K.A.; Sadeghpour, A.; Zhao, S.; Maurya, A.K.; Assaf, K.I.; Moreau, E.; Pauer, R.; Lehner, S.; Jovic, M.; et al. Template-free synthesis of hybrid silica nanoparticle with functionalized mesostructure for efficient methylene blue removal. *Mater. Des.* **2021**, *201*, 109494. [[CrossRef](#)]
20. Putz, A.; Ciopec, M.; Negrea, A.; Grad, O.; Ianăși, C.; Ivankov, O.I.; Milanović, M.; Stijepović, I.; Almásy, L. Comparison of structure and adsorption properties of mesoporous silica functionalized with aminopropyl groups by the co-condensation and the post grafting methods. *Materials* **2021**, *14*, 628. [[CrossRef](#)]
21. Soltani, R.; Marjani, A.; Hosseini, M.; Shirazian, S. Mesostructured hollow siliceous spheres for adsorption of dyes. *Chem. Eng. Technol.* **2020**, *43*, 392–402. [[CrossRef](#)]
22. Moorthy, M.S.; Kim, H.-B.; Sung, A.-R.; Bae, J.-H.; Kim, S.-H.; Ha, C.-S. Fluorescent mesoporous organosilicas for selective monitoring of Hg²⁺ and Fe³⁺ ions in water and living cells. *Micropor. Mesopor. Mater.* **2014**, *194*, 219–228. [[CrossRef](#)]
23. Lee, J.-Y.; Chen, C.-H.; Cheng, S.; Li, H.-Y. Adsorption of Pb(II) and Cu(II) metal ions on functionalized large-pore mesoporous silica. *Int. J. Environ. Sci. Technol.* **2016**, *1*, 65–76. [[CrossRef](#)]
24. Park, S.S.; Moorthy, M.S.; Ha, C. Periodic mesoporous organosilica (PMO) for catalytic applications. *Korean J. Chem. Eng.* **2014**, *31*, 1707–1719. [[CrossRef](#)]
25. Cashin, V.B.; Eldridge, D.S.; Yu, A.; Zhao, D. Surface functionalization and manipulation of mesoporous silica adsorbents for improved removal of pollutants: A review. *Environ. Sci. Water Res. Technol.* **2018**, *4*, 110–128. [[CrossRef](#)]
26. Moorthy, M.S.; Kim, H.-B.; Bae, J.-H.; Kim, S.-H.; Ha, C.-S. Design of core-shell magnetic mesoporous silica hybrids for pH and UV light stimuli-responsive cargo release. *RSC Adv.* **2016**, *6*, 29106–29115. [[CrossRef](#)]
27. Da'na, E. Adsorption of heavy metals on functionalized-mesoporous silica: A review. *Micropor. Mesopor. Mater.* **2017**, *247*, 145–157. [[CrossRef](#)]
28. Santhamoorthy, M.; Thirupathi, K.; Thirumalai, D.; Aldawood, S.; Kim, S.-C. Surface grafted silica adsorbent for efficient removal of Hg²⁺ ions from contaminated water. *Environ. Res.* **2022**, *212*, 113211. [[CrossRef](#)]
29. Ai, K.; Ruan, C.; Shen, M.; Lu, L. MoS₂ nanosheets with widened interlayer spacing for high-efficiency removal of mercury in aquatic systems. *Adv. Funct. Mater.* **2016**, *26*, 5542–5549. [[CrossRef](#)]
30. Santhamoorthy, M.; Thirumalai, D.; Thirupathi, K.; Kim, S.-C. Synthesis of dithiol-modified mesoporous silica adsorbent for selective adsorption of mercury ions from wastewater. *Appl. Nanosci.* **2022**. [[CrossRef](#)]
31. Perdoor, S.S.; Noureddine, A.; Dubois, F.; Man, M.C.; Cattoën, X. Click functionalization of sol-gel materials. In *Handbook of Sol-Gel Science and Technology*; Springer: Cham, Switzerland, 2016. [[CrossRef](#)]
32. Yoshitake, H.; Yokoi, T.; Tatsumi, T. Adsorption behavior of arsenate at transition metal cations captured by amino-functionalized mesoporous silicas. *Chem. Mater.* **2003**, *15*, 1713–1721. [[CrossRef](#)]
33. Heidari, A.; Younesi, H.; Mehraban, Z. Removal of Ni(II), Cd(II), and Pb(II) from a ternary aqueous solution by amino functionalized mesoporous and nano mesoporous silica. *Chem. Eng. J.* **2009**, *153*, 70–79. [[CrossRef](#)]

34. Melnyk, I.V.; Tomina, V.V.; Stolyarchuk, N.V.; Katelnikovas, A.; Kareiva, A. Affordable phosphonic- and phenyl-functionalized silicate adsorbent for metal and dye cations uptake. *J. Porous Mater.* **2022**. [[CrossRef](#)]
35. Moorthy, M.S.; Hoang, G.; Subramanian, B.; Bui, N.Q.; Panchanathan, M.; Mondal, S.; Tuong, V.P.T.; Kim, H.; Oh, J. Prussian blue decorated mesoporous silica hybrid nanocarriers for photoacoustic imaging-guided synergistic chemo-photothermal combination therapy. *J. Mater. Chem. B* **2018**, *6*, 5220–5233. [[CrossRef](#)]
36. Branda, F.; Bifulco, A.; Jehnichen, D.; Parida, D.; Pauer, R.; Passaro, J.; Gaan, S.; Pospiech, D.; Durante, M. Structure and bottom-up formation mechanism of multisheet silica-based nanoparticles formed in an epoxy matrix through an in situ process. *Langmuir* **2021**, *37*, 8886–8893. [[CrossRef](#)] [[PubMed](#)]
37. Hatton, B.; Landskron, K.; Whithall, W.; Perovic, D.; Ozin, G.A. Past, present, and future of periodic mesoporous organosilicas—The PMOs. *Acc. Chem. Res.* **2005**, *4*, 305–312. [[CrossRef](#)]
38. Mather, B.D.; Viswanathan, K.; Miller, K.M.; Long, T.E. Michael addition reactions in macromolecular design for emerging technologies. *Prog. Polym. Sci.* **2006**, *31*, 487–531. [[CrossRef](#)]
39. Moorthy, M.S.; Bharathiraja, S.; Manivasagan, P.; Lee, K.D.; Oh, J. Crown ether triad modified core-shell magnetic mesoporous silica nanocarrier for pH-responsive drug delivery and magnetic hyperthermia applications. *New J. Chem.* **2017**, *41*, 10935–10947. [[CrossRef](#)]
40. Bordoni, A.V.; Lombardo, M.V.; Wolosiuk, A. Photochemical radical thiolene click-based methodologies for silica and transition metal oxides materials chemical modification: A mini-review. *RSC Adv.* **2016**, *6*, 77410–77426. [[CrossRef](#)]
41. Liu, J.; Yang, J.; Yang, Q.H.; Wang, G.; Li, Y. Hydrothermally stable thioether-bridged mesoporous materials with void defects in the pore walls. *Adv. Funct. Mater.* **2005**, *15*, 1297–1302. [[CrossRef](#)]
42. Manivasagan, P.; Bharathiraja, S.; Moorthy, M.S.; Oh, Y.; Seo, H.; Oh, J. Marine biopolymer-based nanomaterials as a novel platform for theranostic applications. *Polym. Rev.* **2017**, *57*, 631–667. [[CrossRef](#)]
43. Saman, N.; Johari, K.; Mat, H. Adsorption characteristics of sulfur-functionalized silica microspheres with respect to the removal of Hg(II) from aqueous solutions. *Ind. Eng. Chem. Res.* **2014**, *53*, 1225–1233. [[CrossRef](#)]
44. Wei, J.; Chen, S.; Li, Y.; He, Z.; Geng, L.; Liao, L. Aqueous Cu(II) ion adsorption by amino functionalized mesoporous silica KIT-6. *RSC Adv.* **2020**, *10*, 20504–20514. [[CrossRef](#)] [[PubMed](#)]
45. Lachowicz, J.I.; Delpiano, G.R.; Zanda, D.; Piludu, M.; Sanjust, E.; Monduzzi, M.; Salis, A. Adsorption of Cu²⁺ and Zn²⁺ on SBA-15 mesoporous silica functionalized with triethylenetetramine chelating agent. *J. Environ. Chem. Eng.* **2019**, *7*, 103205. [[CrossRef](#)]
46. Ryu, S.C.; Naidu, G.; Moon, H.; Vigneswaran, S. Continuous and selective copper recovery by multi-modified and granulated SBA-15. *Chemosphere* **2021**, *271*, 129820. [[CrossRef](#)]
47. Gao, J.; Lei, H.; Han, Z.; Shi, Q.; Chen, Y.; Jiang, Y. Dopamine functionalized tannic-acid-templated mesoporous silica nanoparticles as a new sorbent for the efficient removal of Cu²⁺ from aqueous solution. *Sci. Rep.* **2017**, *7*, 45215. [[CrossRef](#)]
48. Irfai, R.A.; Roto, R.; Aprilita, N.H. Preparation of Fe₃O₄@SiO₂ nanoparticles for adsorption of waste containing Cu²⁺ ions. *Key Eng. Mater.* **2020**, *840*, 43–47. [[CrossRef](#)]
49. Chen, L.; Hao, H.Y.; Zhang, W.T.; Shao, Z. Adsorption mechanism of copper ions in aqueous solution by chitosan–carboxymethyl starch composites. *J. Appl. Polym. Sci.* **2020**, *137*, 48636. [[CrossRef](#)]
50. Su, C.; Berekute, A.K.; Yu, K.-P. Chitosan@TiO₂ composites for the adsorption of copper(II) and antibacterial applications. *Sustain. Env. Res.* **2022**, *32*, 27. [[CrossRef](#)]